Bulletin of Engineering Geology and the Environment (2021) 80:1287–1301
https://doi.org/10.1007/s10064-020-01989-3

ORIGINAL PAPER

Seismic slope stability and failure process analysis using explicit finite element method

Zongyuan Ma[1] · Hongjian Liao[2] · Faning Dang[1] · Yuxiang Cheng[3]

Received: 15 April 2020 / Accepted: 26 September 2020 / Published online: 6 October 2020

Abstract

Earthquake is one of the primary factors that triggers the failure of slopes and the landslides in the mountainous area. In this study, an efficient method for the seismic slope stability analysis and seismic failure process simulation is proposed. The seismic slope stability and the failure process of a two-dimensional slope model are analyzed via the explicit finite element method with the influence of the dynamic mechanical behavior of soil and the frictional resistance characteristic of the slope rupture surface. A dynamic visco-elasto-plastic constituted model for soil is established and written in FORTRAN as a user subroutine of the finite element method code of ABAQUS. The validation of the visco-elasto-plastic constituted model and the explicit finite element method are compared with the experimental results and the implicit method. The seismic factor of safety and the sliding distance of the soil slopes under the natural earthquake conditions are calculated via the dynamic visco-elasto-plastic constituted model and the explicit finite element method. The influence of the ground motion characteristics on the seismic slope stability is analyzed in this study via the specified elastic response acceleration spectrum. The analysis results of this paper suggest that the seismic slope stability analysis and the progressive failure process of the slope under the seismic condition can be analyzed by the explicit finite element method efficiently. The results show that the dynamic mechanical behavior of soil and the ground motion characteristics are both critical influence factors for the seismic slope stability. The frictional resistance characteristic of the slope rupture surface is the principal influence factor for the sliding distance of the slope, and it also has more influence on the sliding distance of a high slope than that of the small slope.

Keywords Earthquake · Seismic slope stability · Slope failure process · Large deformation · Explicit finite element method

Introduction

The ground motion induced by the earthquake is a vital influence factor for the slope stability problem, and many landslides and failure of slopes will be triggered by a strong seismic event in the mountainous area. Landslides are the primary geological disasters which are induced by the earthquake in the mountainous area. These geological disasters can take a heavy toll on the buildings and transportation of the human society, and it may cause economic losses and casualties more than that of the earthquake (Yin et al. 2009; Yin et al. 2011). The loose deposit yield by the landslides will be accumulated in the gully, and it is also the most important source for the geological disaster of debris flow (Tang et al. 2009; Lin et al. 2003).

The process of slope failure and the sliding distance of the slide mass of landslide are two essential influence factors for the damage of landslides. However, the failure process of slope and the sliding distance of the slide mass cannot be well analyzed using the existing methods. The factor of safety (FOS) is an essential parameter to determine the slope or landslide stability, and several methods have been suggested for FOS calculation, including analytical and numerical methods. The limit equilibrium method (LEM) is a general analytical method for the slope stability analysis and FOS calculation,

✉ Zongyuan Ma
mzy_gogo@hotmail.com

[1] State Key Laboratory of Eco-hydraulics in Northwest Arid Region, Xi'an University of Technology, 5 South Jinhua Road, Xi'an 710048, Shaanxi, People's Republic of China

[2] Department of Civil Engineering, Xi'an Jiaotong University, 28 Xianning West Road, Xi'an 710049, Shaanxi, People's Republic of China

[3] College of Geological Engineering and Geomatics, Chang'an University, Middle-section of Nan'er Huan Road, Xi'an 710064, Shaanxi, People's Republic of China

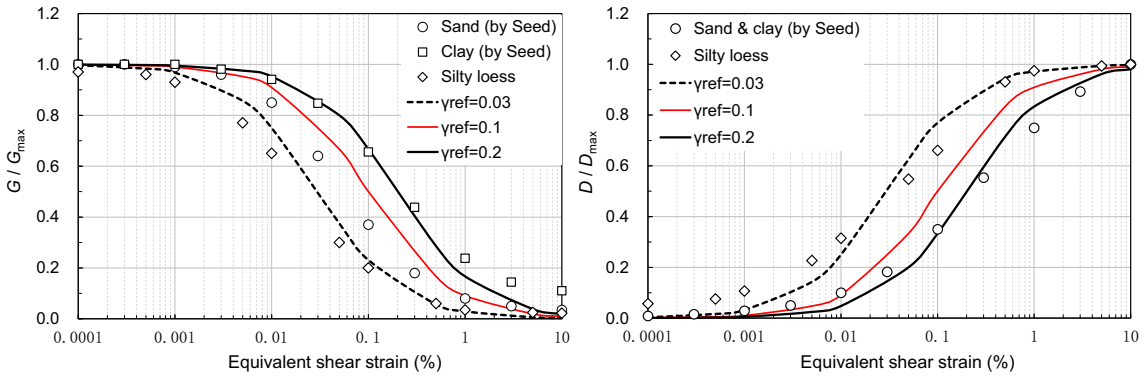

(a) Shear modulus (b) Damping ratio

Fig. 1 Relationship of shear modulus and damping ratio versus equivalent shear strain in % for soil and comparison with the theoretical prediction of Hardin's function

e.g., the circular slip surface method or the general methods of slices (Bishop 1955 and Bishop and Morgenstern 1960; Morgenstern and Price 1965; Spencer 1967; Janbu 1954; Sarma 1979; Fredlund and Krahn 1977). The limit analysis method is a semi-analytic method for the problem of slope stability analysis. The stability of three-dimensional undrained slopes was analyzed by AJ. Li et al. (2009a, 2009b) using the numerical limit analysis method. The FOS of a slope also can be calculated via the numerical method with the strength reduction method (SRM), e.g., finite element method (FEM) or finite difference method (FDM). SRM is a method that the original shear strength parameters (e.g., cohesion c and friction angle φ) of soil mass are divided by the strength reduction factor (SRF) to bring the slope to the point of failure. The shear strength parameters of the soil mass are decreased gradually by SRF until the slope becomes unstable, and the value of SRF when the failure which is initiated is equal to FOS for the slope (Zienkiewicz et al. 1975; Duncan 1996; Dawson et al. 1999). The numerical method has several advantages over the analytical method (e.g., LEM) for slope stability analysis, e.g., finding the critical failure surface automatically. The relationship between the LEM and SRM in slope stability analysis was discussed by Dawson et al. (1999).

The problem of seismic slope stability and the failure process of slope due to earthquakes is rarely investigated. The theory and method for FOS calculation of the static slope stability analysis cannot be applied to the seismic slope stability analysis directly. The pseudo-static method (PSM) is a simplified method for the seismic slope stability analysis. The influence of the earthquake is considered by applying the inertial force to the slope in PSM, and the dynamic process of the earthquake is also neglected in PSM (Leshchinsky and San, 1994; Shukha et al. 2006; Travasarou and Bray 2009). In recent years, some researchers combine PSM with the analytical or numerical method to investigate the seismic slope stability problem (Conte et al. 2000; Nouri et al. 2006; Li et al. 2009a; Bandini et al. 2003). PSM is also applied for the reliability analysis of the seismic slope stability problem (Huang et al. 2018). The possibility of seismic amplification problems in the slopes to be analyzed through two-dimensional

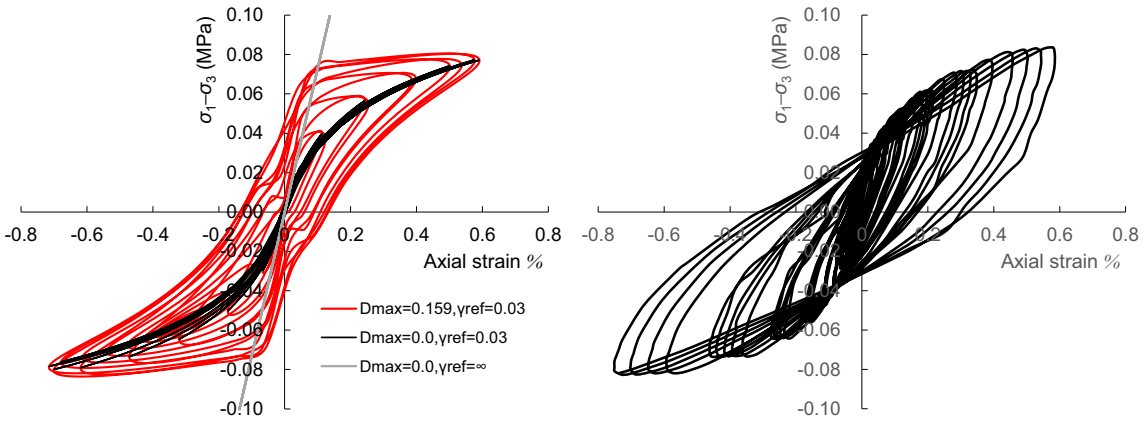

(a) EFEM (b) Experimental results

Fig. 2 Dynamic stress-strain relationship of silty loess predicted by the dynamic visco-elasto-plastic constituted model to compare with dynamic triaxial testing data

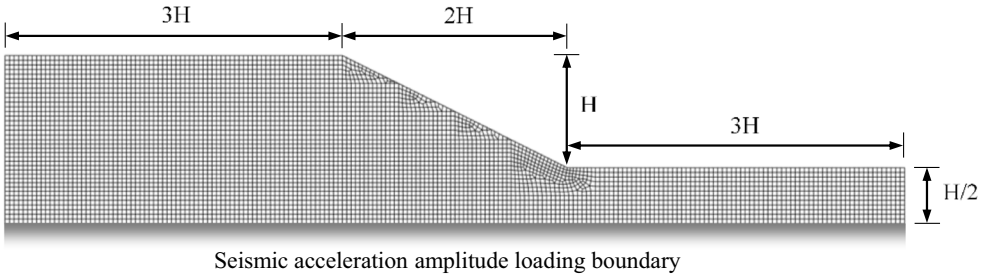

Fig. 3 Dimension and FEM mesh for the slope stability analysis

modeling or two different nonlinear 1-D codes was studied by A. Cavallaro et al. (2008, 2019). The mechanical behavior of geomaterial under the seismic condition is another essential influence factor for the seismic slope stability analysis. However, it has been neglected in the seismic slope stability analysis via PSM and LEM. The detail and the application of PSM are reviewed and discussed by RW. Jibson (2011). In this study, an efficient method for the seismic slope stability and failure process analysis is proposed. The mechanical behavior of soil and the dynamic process induced by the earthquake are taken into account to analyze the seismic slope stability and failure process using the explicit finite element method (EFEM) and SRM.

Theory and method

The explicit dynamics analysis procedure of EFEM is based upon the implementation of an explicit integration rule, and the equations of motion are integrated using the explicit difference integration rule. The nonlinear iterative algorithm in the implicit method is not used in the nonlinear solution of EFEM. The explicit integration of the motion equations through time by using many small-time increments and the solution procedure of EFEM is conditionally stable. The use of small increments is advantageous to the solution of EFEM, and the solution of EFEM can be proceeded without iterations and without requiring tangent stiffness matrices to be formed (Bathe and Wilson 1976). Therefore, the stable computation process and the precise solution will be yielded by EFEM with small timesteps and uniform FEM mesh. EFEM is ideally suited for analyzing high-speed dynamic and large deformation problems (Johnson 2011). The problem of multiphase flow and heat transfer also can be analyzed, simulated, and evaluated via EFEM (Xue et al. 2020, Liu et al. 2020).

A dynamic visco-elasto-plastic constituted model for soil is established in this study to analyze the seismic slope stability problem. The visco-elasto-plastic behavior is predicted by the Kelvin cell in series with a plastic cell corresponding to the Mohr-Coulomb criterion. The visco-elastic stress-strain relation is as follows:

$$\sigma_{ij} = 2G\varepsilon_{ij} + \lambda\varepsilon_v\delta_{ij} + 2\eta_G\dot{\varepsilon}_{ij} + \eta_\lambda\dot{\varepsilon}_v \quad (1)$$

where K and G are the bulk and shear modulus, and η_K and η_G are the dynamic viscosity for volume and shear deformation.

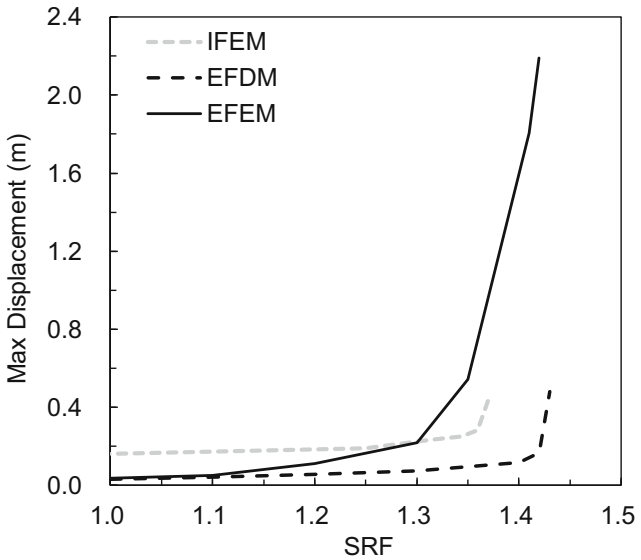

Fig. 4 Relationship of maximum displacement of slope versus SRF yield by different methods

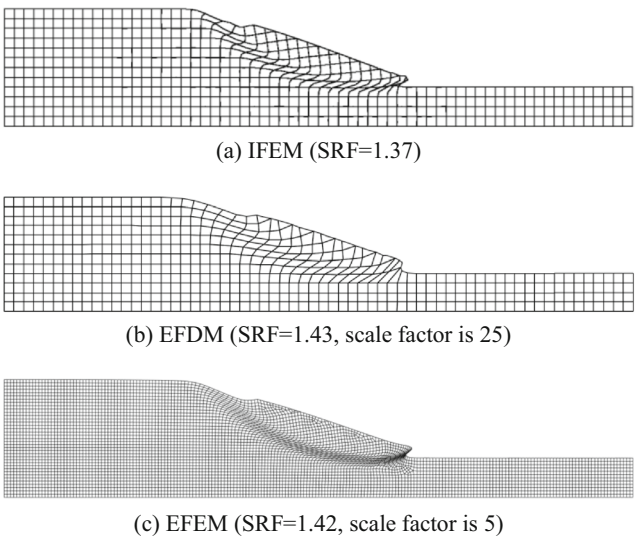

Fig. 5 Comparison of FEM mesh deformation calculated by IFEM, EFDM, and EFEM with $H = 30$ m

Table 1 Soil parameters used in the various analysis section

Section	G_{max} (MPa)	Poisson's ratio ν	γ_{ref}	D_{max}	c (kPa)	φ (°)
Comparison	29.2	0.2	0.03	0.159	–	–
Static	40	0.25	∞	0.0	30	20.0
Seismic	40	0.25	0.1	0.2	30	20.0

The values of η_K and η_G are determined by the following formula (Clough and Penzien 1975):

$$\eta_G = \frac{2GD}{2\pi f}, \eta_K = \frac{2KD}{2\pi f} \tag{2}$$

where D is the damping ratio, and f is the frequency of the structure. The following function for the relationship of the shear modulus reduction versus cyclic shear strain was suggested by Hardin and Drnevich (1972a, 1972b):

$$G/G_{max} = 1/(1 + \gamma/\gamma_{ref}) \tag{3}$$

$$D/D_{max} = (\gamma/\gamma_{ref})/(1 + \gamma/\gamma_{ref}) \tag{4}$$

where γ_{ref} is reference shear strain, and the shear modulus and damping ratio reduction factor G/G_{max} and D/D_{max} are 0.5 when $\gamma = \gamma_{ref}$. Figure 1 shows the relationship of the shear modulus reduction versus equivalent shear strain in % for sand (Seed et al. 1986), clay (Sun et al. 1988), and silty loess (this study) compared with the theoretical prediction of the Hardin's function. The mechanical behavior of soil would be linear elastoplasticity (no dynamic characteristics of soil will be taken into account) if the reference shear strain $\gamma_{ref} \to \infty$ and the damping ratio $D = 0$. The shear modulus of the soil will be decreased rapidly if the value of γ_{ref} is small. The dynamic parameters of the soil for seismic slope stability analysis in this study are as follows: the reference shear strain $\gamma_{ref} = 0.1$, and the maximum damping ratio $D_{max} = 0.2$.

Compare with the equivalent linear method (Schnabel et al. 1972), the analysis procedure of the dynamic constituted model for soil via EFEM is entirely nonlinear. A verification example of the soil dynamic stress-strain relationship is calculated using one 4-node plane strain and reduced integration element. A sine acceleration amplitude is loaded in the vertical direction of the element, and another vertical direction is fixed. The function of the sine acceleration amplitude is as follows:

$$A = \frac{t^{10}}{2.25 \times 10^6 e^t} \sin(2\pi t) \tag{5}$$

where A is the value of acceleration amplitude, t is the vibration time, and the maximum acceleration of the sine amplitude is 0.2 m/s^2. A dynamic triaxial test result of the silty loess from the loess plateau in the northwest of China is used to compare with the dynamic stress-strain relationship predicted by the dynamic visco-elasto-plastic constituted model proposed by this paper (see Fig. 2). The properties of the silty loess are as follows: the maximum shear modulus $G_{max} = 29.2$ MPa, the maximum damping ratio $D_{max} = 0.159$, the reference shear strain $\gamma_{ref} = 0.03$, and the Poisson's ratio $\nu = 0.2$. A sine wave with frequency $f = 1.0$ is also used in the dynamic triaxial test. The stress-strain relationship predicted by the dynamic visco-elasto-plastic constituted model shows that no hysteresis loop phenomenon appears in the dynamic mechanical behavior of soil if the damping ratio $D_{max} = 0.0$, and the linear elastic stress-strain relationship will be yielded if reference shear strain $\gamma_{ref} \to \infty$. Thus, the dynamic characteristics of soil will be neglected, and the mechanical behavior of soil is linear elastic if the damping ratio $D = 0$ and the reference shear strain $\gamma_{ref} \to \infty$.

The undrained cyclic laboratory behavior of sandy soils by cyclic triaxial tests was studied by F. Castelli et al. (2019). The level of strain is studied by P. Capilleri et al. (2014) and F. Castelli et al. (2016) using resonant column tests and cyclic torsional shear tests. The FOS of the soil slope is calculated via SRM in this study. The same factor SRF is applied to both of the shear strength parameters (c and φ) and dynamic parameters of the soil (D_{max} and γ_{ref}). The dynamic soil property also reduced by the same factor SRF, which is applied to the shear strength parameters of the soil. The reduced strength parameters (c_f and φ_f) and dynamic parameters (G_{max} and

Table 2 The main characteristics of the input earthquake motions

Earthquake record	Imperial Valley (USA)	Kobe (Japan)	Loma Prieta (USA)	Kocaeli (Turkey)
Recording station	USGS station 5115	Kakogawa (CUE90)	CDMG station 47,381	Yarimca (KOERI330)
Date of occurrence	Oct. 15, 1979	Jan. 16, 1995	Oct. 18, 1989	Aug. 17, 1999
Significant duration (s)	8.92	12.86	11.37	15.62
Max. acceleration (g)	0.315	0.345	0.367	0.349

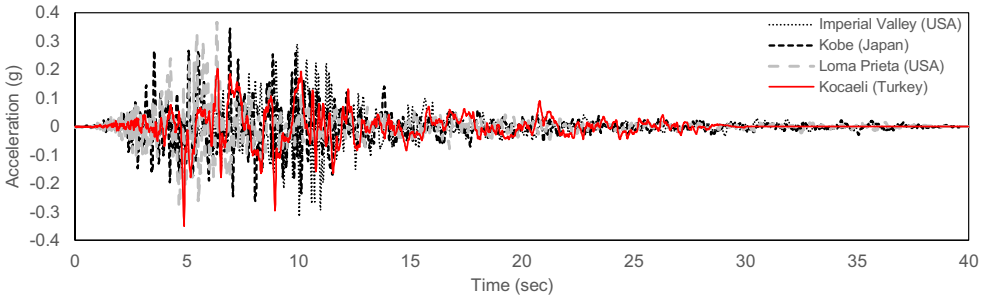

Fig. 6 Seismic acceleration amplitudes obtained from four earthquake events

γ_{ref}) are given by

$$c_f = \frac{c}{\mathrm{SRF}},\quad \varphi_f = \arctan\left(\frac{\tan\varphi}{\mathrm{SRF}}\right),\quad G_{\max f} = \frac{G_{\max}}{\mathrm{SRF}},\quad \gamma_{\mathrm{ref}f} = \frac{\gamma_{\mathrm{ref}}}{\mathrm{SRF}} \tag{6}$$

The dynamic visco-elasto-plastic constituted model for soil is written in FORTRAN as a user subroutine and loaded into the finite element method code of ABAQUS with the subroutine interface VUMAT of EFEM module (Simulia 2017). Comparing with the equivalent linear method (Schnabel et al. 1972), the dynamics analysis procedure of the dynamic constituted model for soil via EFEM is entirely nonlinear. The stability and failure process of the two-dimensional plane-strain soil slope is analyzed, the slope magnitude (height/run) is 1:2, and the dimension and FEM mesh of the slope are shown in Fig. 3. The acceleration due to gravity is set to 9.81 m/s^2 in this study, and the large deformation model is used in EFEM calculations. The elastic properties of the soil are as follows: Young's modulus $E = 100.0$ MPa, Poison ratio $\nu = 0.25$, and unit weight $\gamma = 20.0$ kN/m^3. The soil's strength parameters of the slope are as follows: cohesion $c = 30$ kPa, and friction angle $\varphi = 20.0°$. The initial gravity field is established before the seismic slope stability analysis. The slope stability problem in two-dimensional plane strain and static condition with $H = 30$ m and nonassociated flow rule (dilation angle $\psi = 0$) is analyzed using the implicit finite element method (IFEM) and explicit finite difference method (EFDM) to compare with the results yield by EFEM. The FEM code of ABAQUS, the slope stability analysis code of SLOPE64 (Griffiths and Lane 1999; Griffiths 2015), and the FDM code of FLAC (ITASCA 2015) are used for EFEM, IFEM, and EFDM calculation respectively. The dynamic characteristics of soil are not considered ($\gamma_{ref} \to \infty$ and $D = 0$) in the static slope stability analysis. The relationship of maximum displacement of slope versus SRF yield by the different methods is shown in Fig. 4. A comparison of FEM mesh deformation calculated by IFEM, EFDM, and EFEM is shown in Fig. 5.

The deformation of the slope calculated by EFEM (large deformation model) is larger than that of IFEM and EFDM (small deformation model). The slope cannot be brought to complete failure by SRM and EFEM in the static condition. However, the calculation of slope stability using IFEM will be stopped due to non-convergence of the nonlinear iterations when the slope is brought to failure by SRM. So, the non-convergence option is a suitable indicator of the slope failure, and the values of FOS can be easily determined by this criterion when the slope stability is analyzed using IFEM under static conditions. However, it is difficult to determine the failure of slope and the values of FOS under static conditions (neglect the dynamic characteristics of the soil) via EFEM. In this study, the phenomenon of sustained deformation of the slope during the calculation is taken as an indicator of failure for FOS determination of seismic slope stability analysis. Soil parameters and its values used in the various analysis sections are shown in Table 1.

Seismic slope stability analysis

The failure process of a soil slope under the seismic condition with the dimension $H = 30$ m is analyzed via EFEM. The seismic acceleration amplitudes are used to simulate the seismic load of the earthquake. The vertical and horizontal

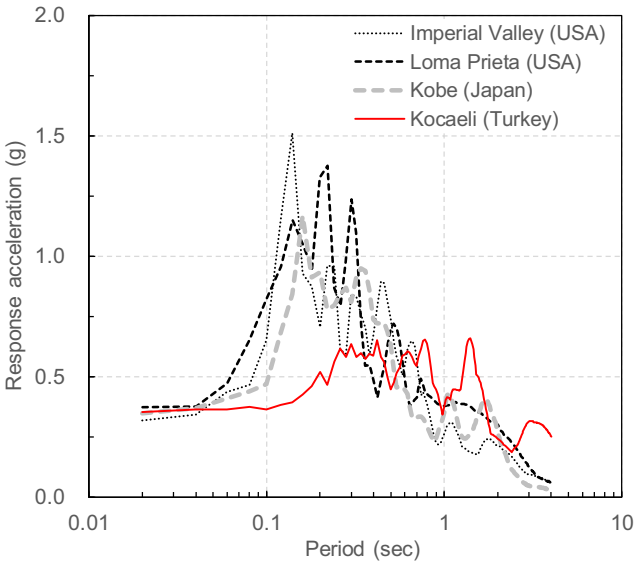

Fig. 7 Elastic response acceleration spectra (damping value is 5%) of four earthquake events

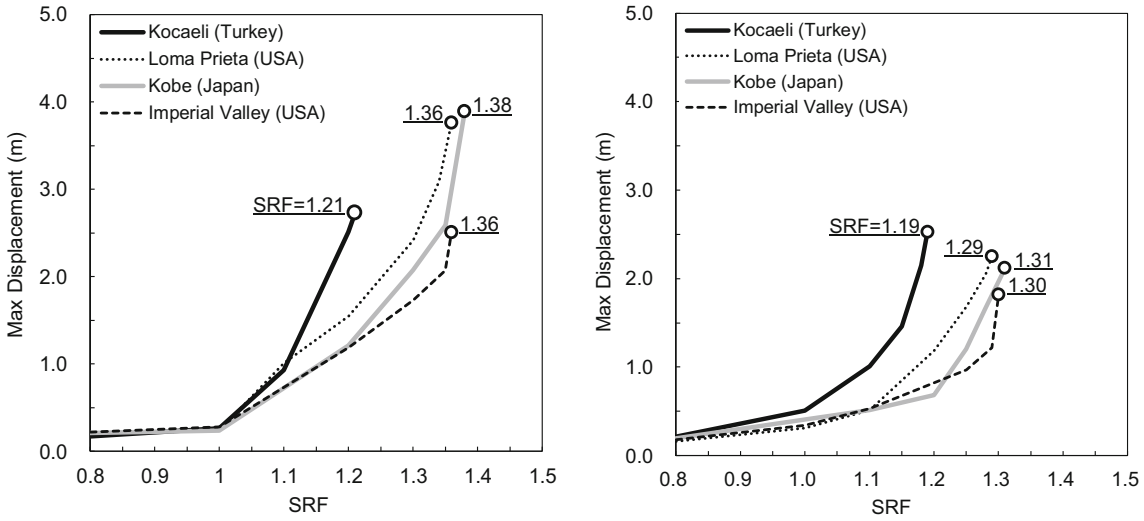

(a) Associated flow rule ($\varphi = \psi$) (b) Nonassociated flow rule ($\psi = 0$)

Fig. 8 Relationship of maximum displacement of the slope due to different earthquake events versus SRF with associated and nonassociated flow rule

components of the seismic boundary condition are both set to the same acceleration amplitude and loaded on the bottom boundary of the slope (shown in Fig. 3). The two lateral boundaries of the slope are set to the zero-acceleration boundary. The initial gravity field is established before the seismic slope stability analyses. Four seismic acceleration amplitudes obtained from four earthquake events are used to analyze the problem of slope seismic failure process, respectively. The four earthquake events are as follows: the Imperial Valley earthquake (USA 1979), the Loma Prieta earthquake (USA 1989), the Kobe earthquake (Japan 1995), and the Kocaeli earthquake (Turkey 1999) (Seismosoft 2016), and the acceleration amplitudes are shown in Fig. 6. The elastic response acceleration spectra of the four earthquake events with 5% damping value are shown in Fig. 7. The four seismic acceleration amplitudes have similar peak acceleration but have different elastic response acceleration spectra and ground motion characteristics. The peak response period T_g of the Kocaeli earthquake acceleration amplitude is larger than that of the others, but the maximum response acceleration β_{max} of the Kocaeli earthquake response spectrum is lower than that of the others significantly. The main characteristics of the input earthquake motions are shown in Table 2.

The contact interaction behavior is considered in this study to investigate the influence of the frictional characteristic of the slope rupture surface on the sliding distance of the slide

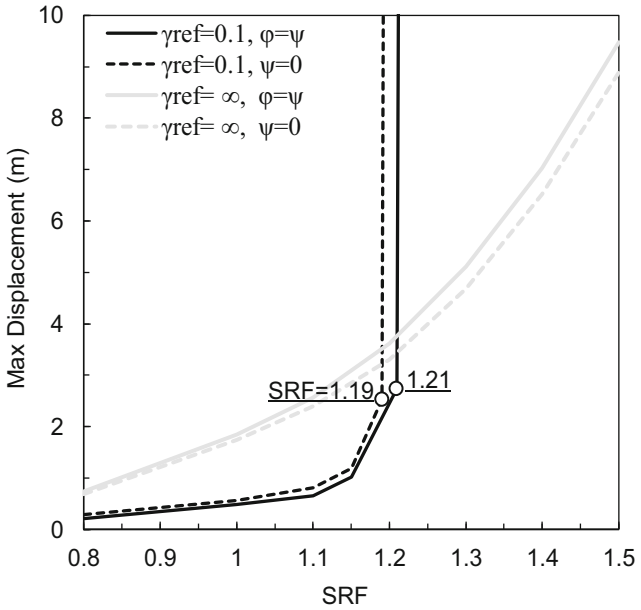

Fig. 9 Relationship of maximum displacement of the slope due to Kocaeli earthquake versus SRF with different values of γ_{ref}

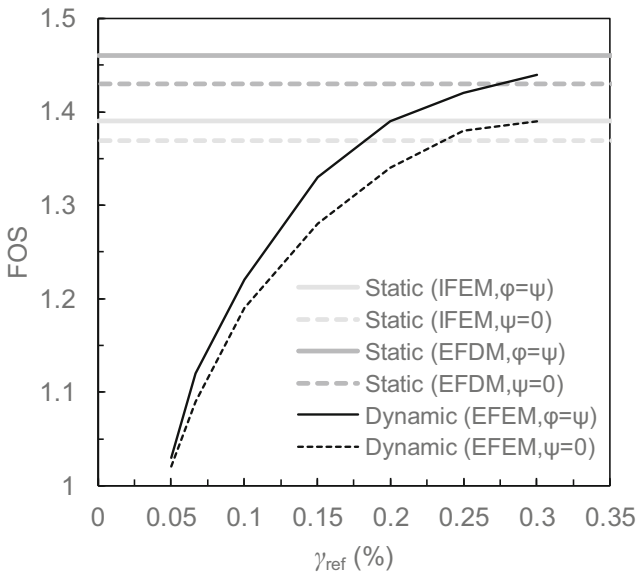

Fig. 10 FOS of slope yield by EFEM, IFEM, and EFDM with different values of γ_{ref}

mass. The interior elements contact interaction technology and Coulomb's law of friction are used to simulate the contact behavior of the slope rupture surface. The normal and shear contact stiffness is both rigid; i.e., the friction coefficient μ is the unique friction parameter in this study. The element deletion technology is used to remove the distort element in the process of seismic analysis, and the rupture surface and sliding process of the slope can be calculated by this method. The relationship of the maximum displacement of the slope due to the different earthquake events versus SRF is shown in Fig. 8. The data points (labeled with the values of SRF) of the curves in Fig. 8 are the last points before the slope sliding; i.e., the values of SRF of those points are the values of seismic FOS of the slope. The results yielded by the seismic slope stability analysis show that the values of FOS under the Kocaeli earthquake are smaller than that of the others. It indicates that the characteristic of the ground motion (response spectrum) has a positive influence on the seismic slope stability. Figure 9 shows the relationship of the maximum displacement of slope with $H = 30$ m due to the Kocaeli earthquake versus SRF with different values of the reference shear strain γ_{ref}. The displacement of the slope is increased with the increase of the values of SRF. However, the failure of the slope does not appear if the characteristics of soil dynamics are neglected ($\gamma_{ref} \rightarrow \infty$ and $D = 0$) in the seismic slope stability analysis. This phenomenon indicates that the dynamic mechanical behavior of soil must be considered in the seismic slope stability analysis. The values of seismic FOS of the slope yield by EFEM (ABAQUS) with the Kocaeli earthquake amplitude and different values of γ_{ref} compared with the values of static FOS of slope yield by IFEM (SLOPE64) are shown in Fig. 10. The value of seismic FOS of the slope is close to the static FOS of the slope when the value of γ_{ref} is fairly large, and the value of seismic FOS of the slope decreases as the value of γ_{ref} decreases. As mentioned above, the reference shear strain γ_{ref} is an essential parameter for the seismic stability analysis of the slope, and the earthquake will have few influences on the slope stability if the dynamic characteristics of soil are neglected ($\gamma_{ref} \rightarrow \infty$) in the seismic analysis of the slope.

Horizontal displacement, velocity, and acceleration response of the slope crest versus the seismic duration (Kocaeli earthquake) with different values of SRF are shown in Figs. 11, 12, and 13, respectively. The slope velocity response during the earthquake shows that the velocity of slide

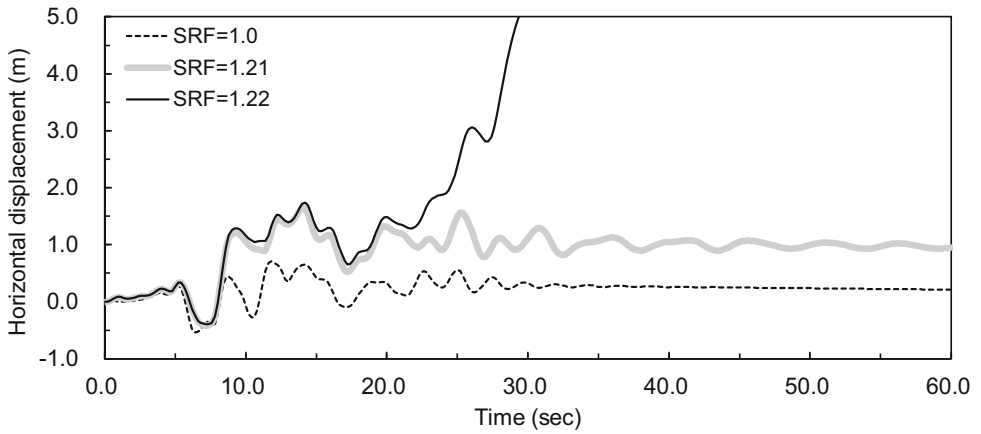

(a) Associated flow rule ($\varphi = \psi$)

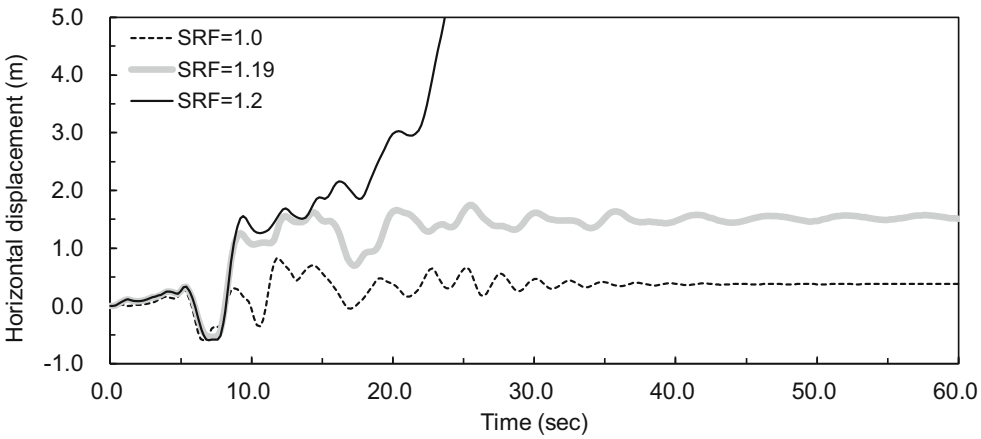

(b) Nonassociated flow rule ($\psi = 0$)

Fig. 11 Horizontal displacement of slope crest versus seismic duration (Kocaeli earthquake) with different values of SRF

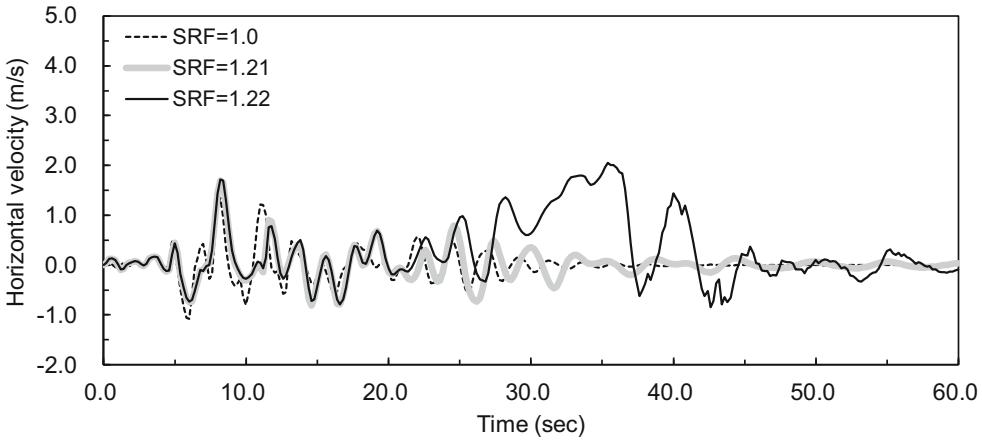

(a) Associated flow rule ($\varphi = \psi$)

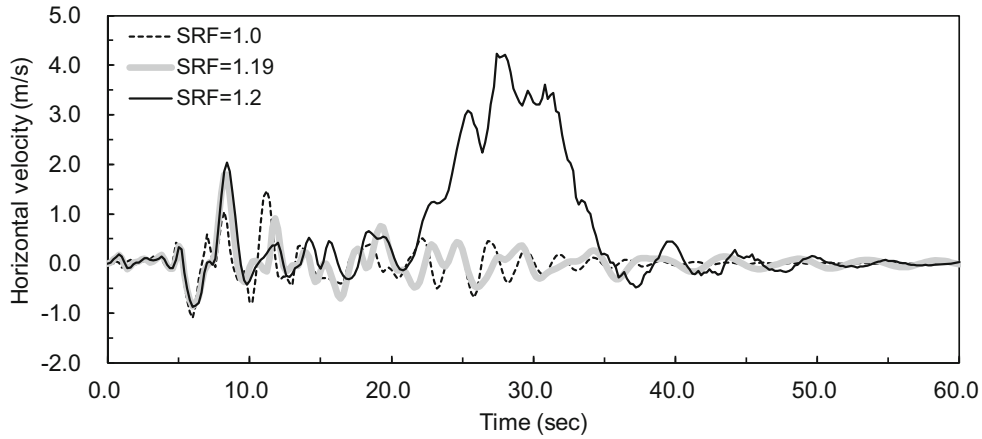

(b) Nonassociated flow rule ($\psi = 0$)

Fig. 12 Horizontal velocity of slope crest versus seismic duration (Kocaeli earthquake) with different values of SRF

mass has a significant increase when the failure of the slope has occurred, and the slide mass comes to slow down due to the frictional resistance and decrease of the gravitational potential energy. The slope acceleration response during the earthquake shows that the acceleration response amplitude of the slope crest has a high-frequency fluctuation when the failure of the slope has occurred, and the slide mass will speed up to slip. The mesh deformation, displacement contour, and velocity contour of the slope during the seismic process of Kocaeli earthquake with associated flow rule ($\varphi = \psi$) and nonassociated flow rule ($\psi = 0$) when the slope is brought to failure by SRM are shown in Figs. 14 and 15. The computation results show that the failure of the slope under the seismic condition is a progressive failure process, and different slip surface and failure mechanism of the slope are yielded by associated ($\varphi = \psi$) and nonassociated flow rule ($\psi = 0$).

The frictional resistance characteristic of the slope rupture surface is a crucial influence factor for the sliding distance D of the slide mass. In actual situations, the frictional resistance characteristic of the slope rupture surface is influenced by several factors, such as water, air, and thermal decomposition (Goren et al. 2010). The seismic slope stability analysis with $H = 30$ m, SRF = 1.20, $\psi = 0$, and different values of μ is processed to investigate the influence of frictional resistance characteristic of the slope rupture surface on the sliding distance of the slide mass. The mesh deformation of the slope due to the seismic process of Kocaeli earthquake with different values of friction coefficient μ is shown in Fig. 16.

The calculation results show that the sliding distance of the slide mass after the earthquake is influenced by the friction coefficient μ significantly. The maximum value of the sliding distance D approaches the slope height if the value of friction coefficient μ between $0.1 \sim 0.2$. A short sliding distance is yielded, and the main body of the slide mass is still laying on the slope after the failure of the slope if the value of friction coefficient μ is larger than 0.2. The seismic response (horizontal acceleration, velocity, and displacement) of the slope crest versus the seismic duration with different values of

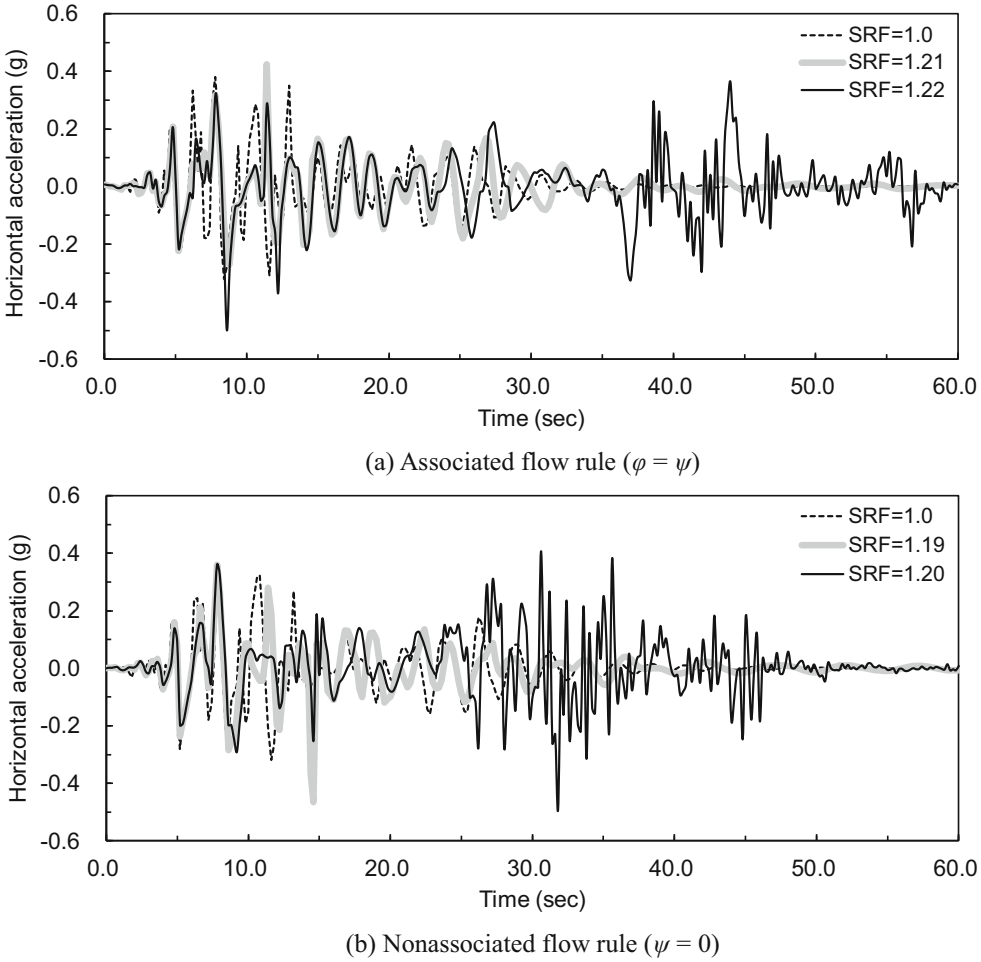

Fig. 13 Horizontal acceleration of slope crest versus seismic duration (Kocaeli earthquake) with different values of SRF

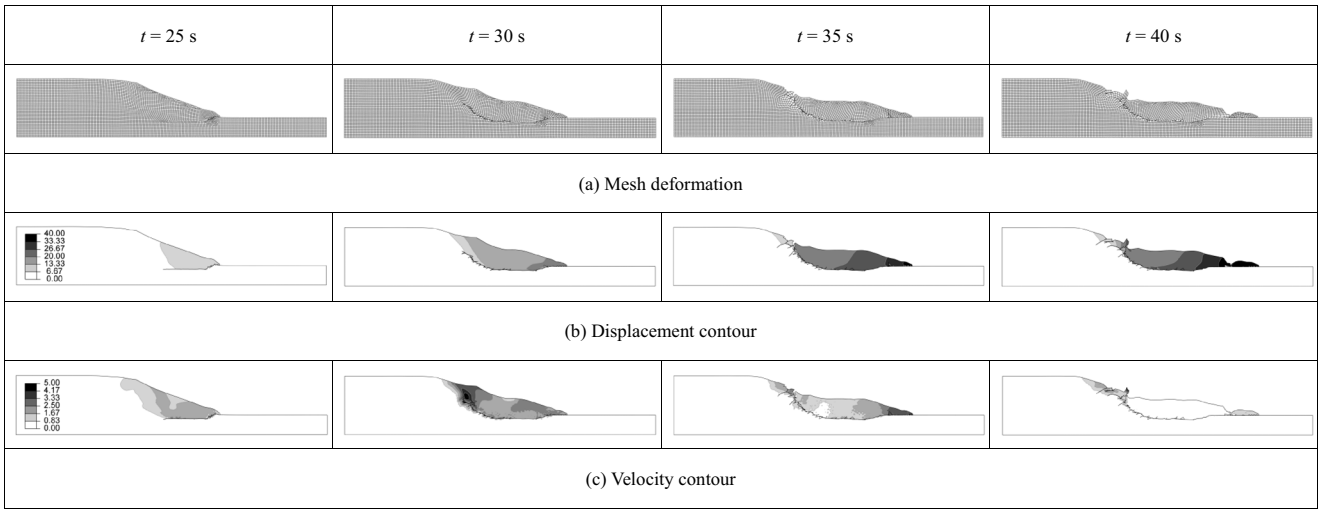

Fig. 14 State of slope during the seismic process of Kocaeli earthquake (scale factor is 1.0) with the values of SRF = 1.23 and associated flow rule ($\varphi = \psi$)

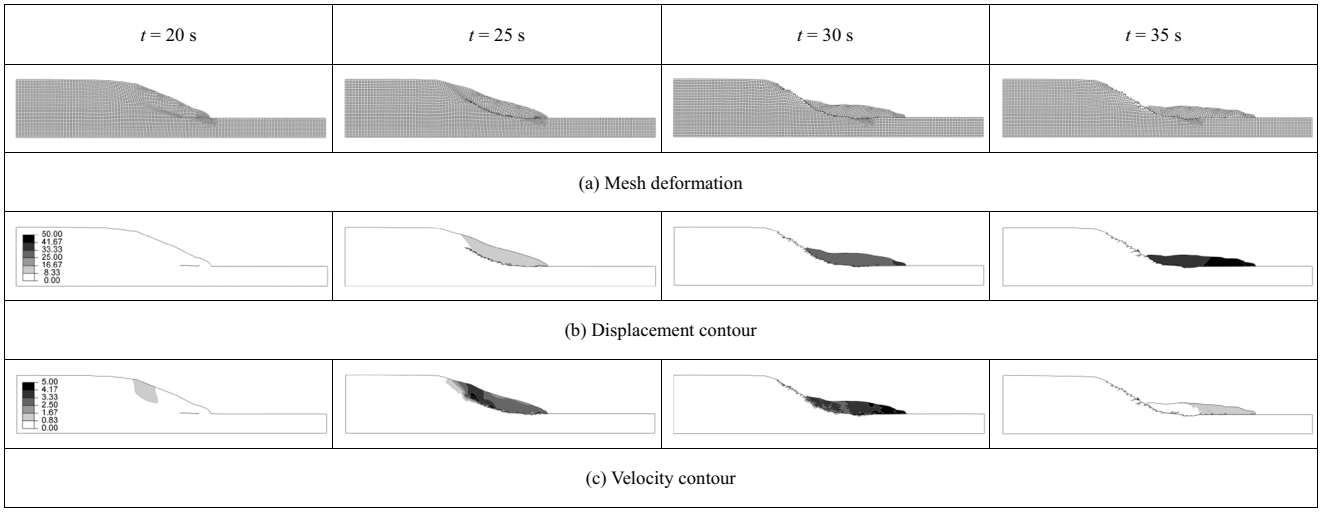

Fig. 15 State of slope during the seismic process of Kocaeli earthquake (scale factor is 1.0) with the values of SRF = 1.20 and nonassociated flow rule ($\psi = 0$)

friction coefficient μ is shown in Fig. 17. The acceleration response amplitude of the slide mass with low frictional resistance characteristic has more significant fluctuation than that of the high resistance characteristic when the slope is sliding. The value of the slip velocity of the slide mass with low frictional resistance characteristic is higher than that of the high resistance characteristic.

The values of slope sliding distance D calculated with the different values of friction coefficient μ are shown in Table 2, and the relationship of slope sliding distance D/H versus values of friction coefficient μ is shown in Fig. 18. The maximum slope sliding distance is decreased significantly with increasing values of the friction coefficient μ. However, the high slope still yields a large sliding distance due to earthquake than that of the small slope with a high frictional resistance characteristic of the slope rupture surface. The relationship of D/H versus μ shows that the frictional resistance characteristic of the slope rupture surface has more influence on the sliding distance of a high slope than that of a small slope. The values of slope sliding distance with different values of friction coefficient are shown in Table 3.

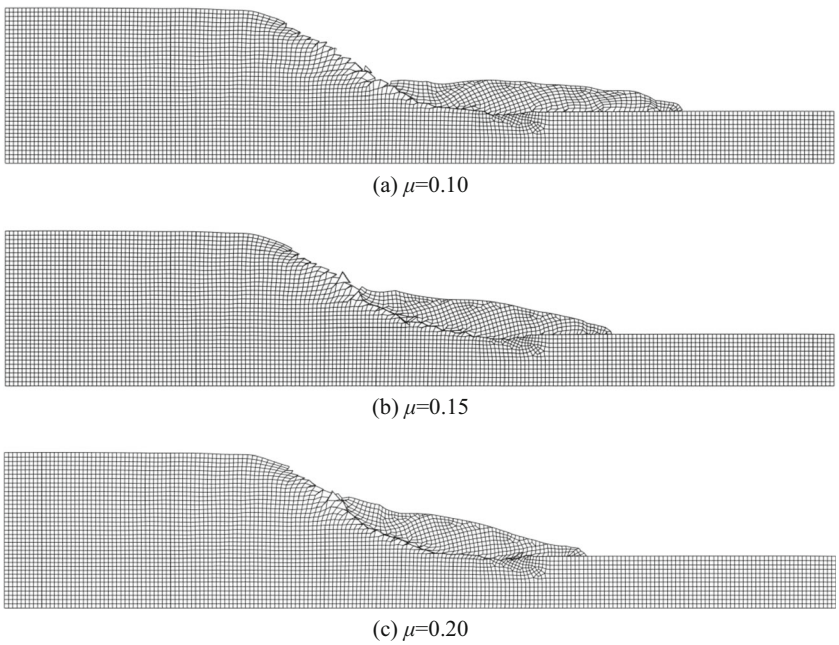

Fig. 16 Mesh deformation of slope due to seismic process of Kocaeli earthquake (scale factor is 1.0) with different values of friction coefficient μ

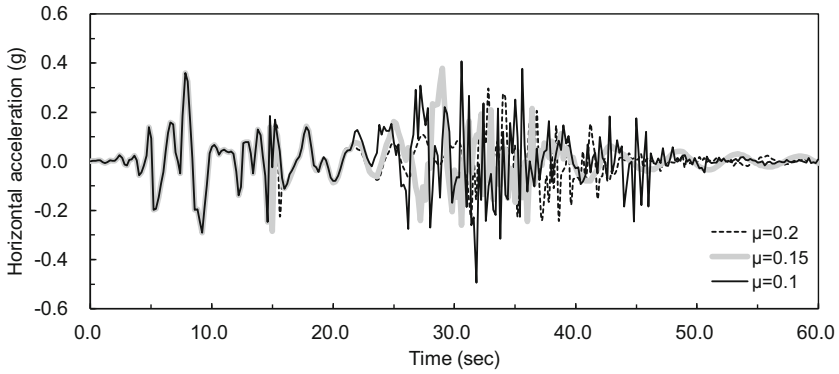

(a) Horizontal acceleration

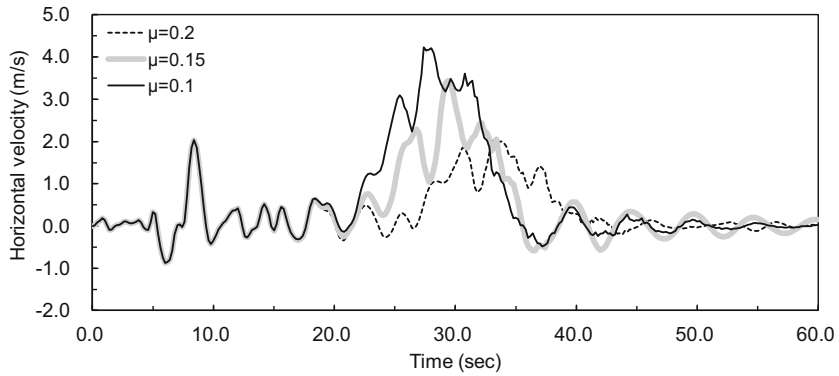

(b) Horizontal velocity

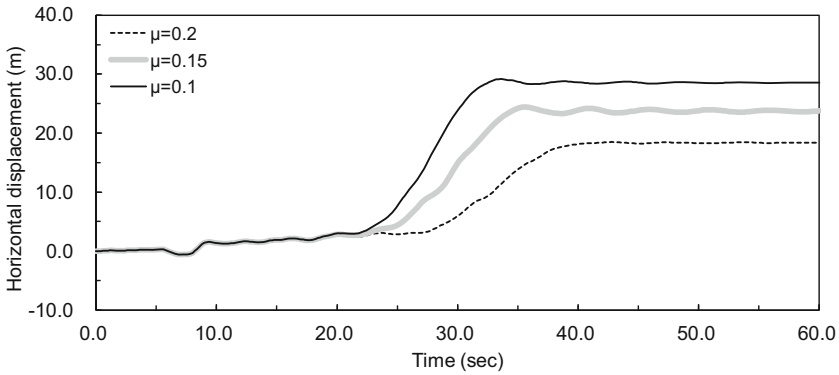

(c) Horizontal displacement

Fig. 17 Seismic response of slope crest versus seismic duration with different values of friction coefficient μ

Table 3 The values of slope sliding distance D with different values of friction coefficient μ (m)

Friction coefficient μ Height of the slope H (m)	0.1	0.15	0.2	0.3
30	51.92	32.26	24.47	19.78
50	91.12	65.53	51.64	49.76
100	284.66	181.01	131.81	128.32

Influence of ground motion characteristics on seismic slope stability

The specified segment response acceleration spectrum is used to create the artificial seismic acceleration amplitudes. The influence of the ground motion characteristics (T_g and A_{max}) on seismic FOS of the slope is analyzed via the artificial seismic acceleration amplitudes and nonassociated ($\psi = 0$) flow rule. The specified elastic response acceleration spectrum with 5% damping value and its fitting curve for the artificial

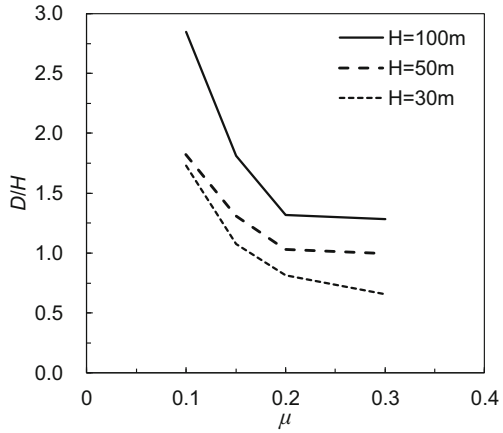

Fig. 18 Relationship of slope sliding distance D/H versus values of friction coefficient μ

seismic acceleration amplitude creation are shown in Fig. 19. The descent section of the segment response acceleration spectrum is predicted by the function as follows (State Economic and Trade Commission, PRC 2000):

$$\beta = \beta_{\max}\left(T_g/T\right)^{0.6} \tag{7}$$

where β is the response acceleration of a single degree of freedom elastomer with 5% damping value, $\beta_{\max}$ is the peak response acceleration, T_0 is the starting point of the peak response stage ($T_0 = 0.1$ s in this study), and T_g is the peak response period (Newmark and Hall 1982; Gupta 1990). Several artificial seismic acceleration amplitudes are created using the computer code SIMQKE_GR (Piero 2012) with

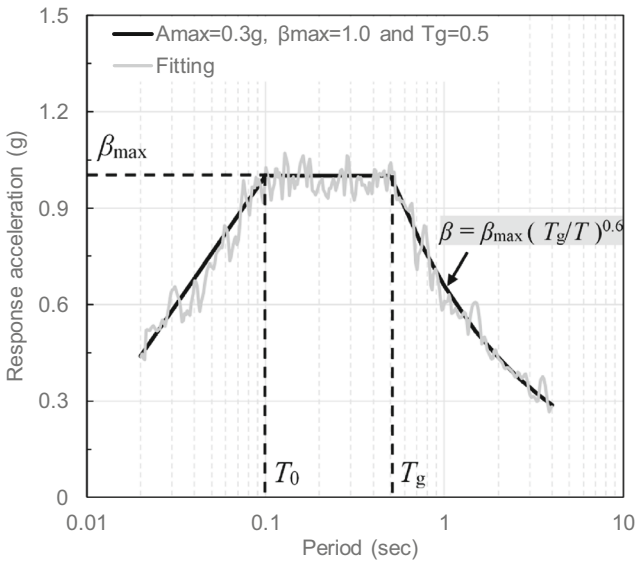

Fig. 19 Artificial specified elastic response acceleration spectrum (damping value is 5%) and its fitting curve for artificial seismic acceleration amplitude creation

different peak response period T_g and peak acceleration $A_{\max}$ via fitting the artificial specified elastic response acceleration spectrum (shown in Fig. 19). The artificial seismic acceleration amplitudes are shown in Fig. 20.

The relationship of the seismic FOS of the slope versus the different values of response spectrum characteristic (T_g and $A_{\max}$) is shown in Fig. 21. The influence of response spectrum characteristics (T_g and $A_{\max}$) on the seismic FOS of the slope with the height of 30 m and 50 m is shown in Fig. 21. The values of the FOS are decreased with the increase of the values of T_g and $A_{\max}$, but the peak response period T_g has more impact on the seismic stability of slopes. Therefore, the failure risk of the slope under the seismic condition will be increased significantly if a long peak response period and high acceleration earthquake event have occurred. The seismic displacement response of slope due to the earthquake is increased with the increased value of the coefficient $\beta_{\max}$. However, the peak response acceleration $\beta_{\max}$ of the response spectrum has few influences on the seismic slope stability. A comparison of the results obtained by the EFEM (peak acceleration $A_{\max} = 0.3$ g) and PSM (horizontal inertia force $A_h = 0.3$ g) shows that the values of FOS yielded by the EFEM is close to that of PSM if the peak response period of the earthquake T_g is very long. In other words, the results of the slope stability analysis obtained by PSM could be conservative due to the neglection of the dynamic process of the earthquake and the mechanical behavior of geomaterial.

Conclusion

The dynamic mechanical behavior of soil and the ground motion characteristics are considered to analyze the seismic slope stability problem using EFEM. An efficient method to analyze the slope stability and progressive failure process under seismic condition is proposed in this paper. The following conclusions can be stated:

IFEM has more advantages than EFEM in static slope stability analysis. However, the seismic stability and the progressive failure process of the slope under the seismic condition can be predicted using EFEM more efficiently. The dynamic mechanical behavior of soil has a significant influence on the seismic stability of the soil slopes. The failure of a soil slope due to a seismic event has a strong relationship with the strength and dynamic mechanical behavior of soil, and the seismic FOS of the soil slope should be determined by both of the strength and dynamic parameters of soil. The seismic FOS of the slope

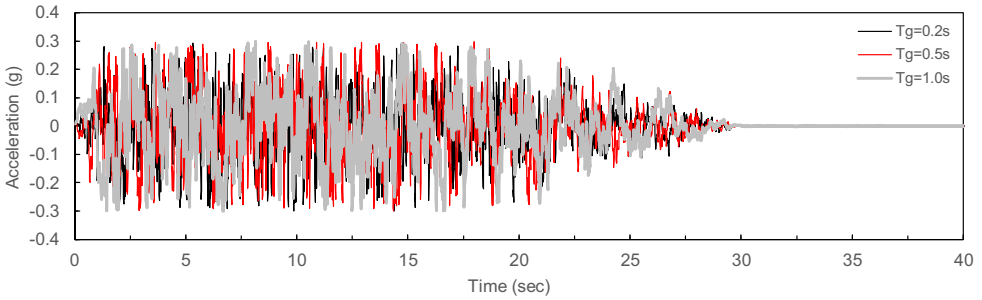

(a) with different values of T_g (A_{max}=0.3g)

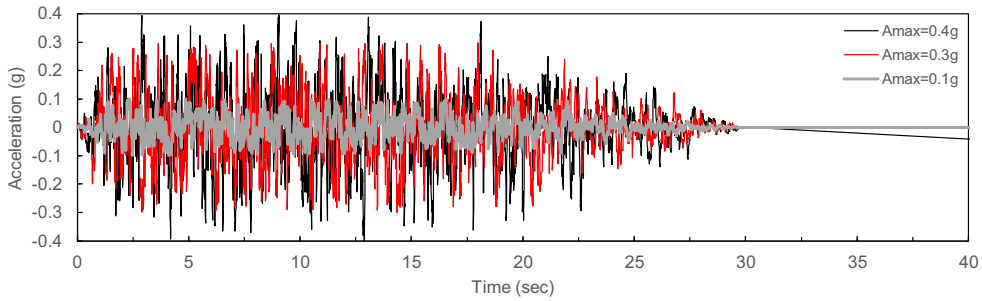

(b) with different values of A_{max} (T_g=0.5s)

Fig. 20 Artificial seismic acceleration amplitudes with different peak response period T_g and peak acceleration A_{max}

cannot be yielded via SRM if the dynamic mechanical behavior of the soil is neglected.

Moreover, the frictional resistance characteristic of the slope rupture surface is the principal influence factor for the seismic failure process and sliding distance of the slope, and the frictional resistance characteristic has more influence on the sliding distance of a high slope than that of a small slope.

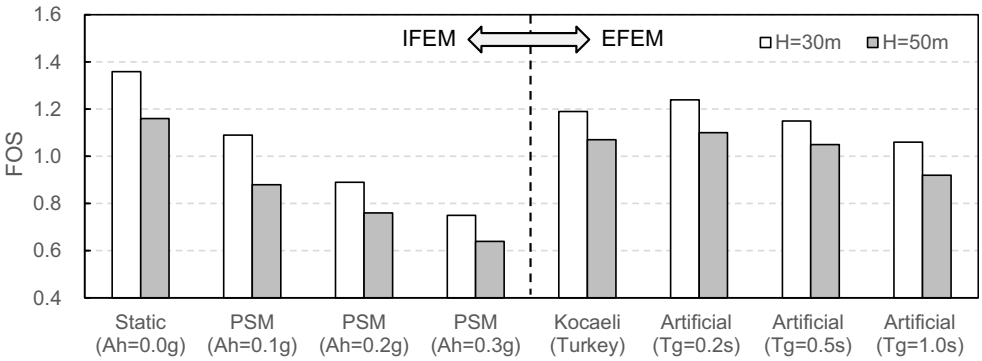

(a) Peak response period T_g (A_{max}=0.3g)

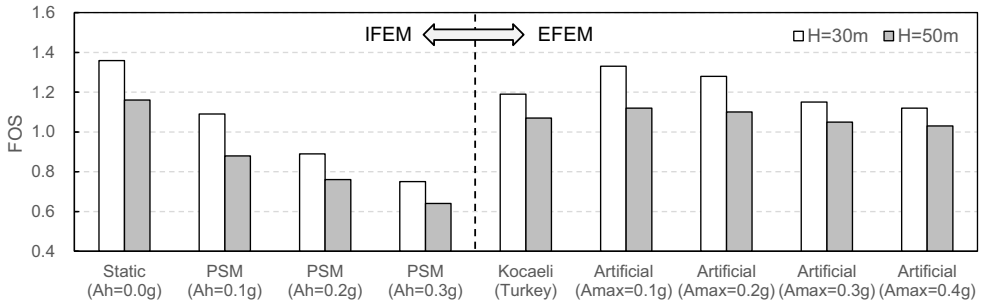

(b) Peak acceleration A_{max} (T_g=0.5s)

Fig. 21 Influence of characteristic of response spectrum on seismic FOS of slope with various slope height and nonassociated ($\psi = 0$) flow rule

The slope will have more seismic failure risk if the ground motion has a long peak stage duration and high acceleration magnitude. The prediction and evaluation of the potentially affected area for the landslides disaster also can be analyzed via the way suggested in this paper. Future research works will further investigate the seismic failure process of the soil slope in three dimensions.

Funding The research described in this paper was funded by the National Natural Science Foundation of China (No. 41630639, 51879212). The first author of the paper received scholarship (CSC NO. 201808615023) from the Chinese Scholarship Council (CSC) to conduct the research described in this paper at Colorado School of Mines.

References

Bandini P, Salgado R, Loukidis D (2003) Stability of seismically loaded slopes using limit analysis. Géotechnique. 53(5):463–479

Bathe KJ, Wilson EL (1976) Numerical methods in finite element analysis. Prentice-Hall Inc., Englewood Cliffs

Bishop AW (1955) The use of the slip circle in the stability analysis of slopes. Géotechnique. 5(1):7–17

Bishop AW, Morgenstern N (1960) Stability coefficients for earth slopes. Géotechnique. 10(4):164–169

Capilleri P, Cavallaro A, Maugeri M (2014) Static and dynamic characterization of soils at Roio Piano (AQ). Italian Geotechnical Journal. 48:38–52

Castelli F, Cavallaro A, Grasso S, and Ferraro A (2016) In situ and laboratory tests for site response analysis in the ancient city of Noto (Italy). Proceedings of the 1st IMEKO TC4 International Workshop on Metrology for Geotechnics, Benevento, 85–90

Castelli F, Cavallaro A, Grasso S, and Lentini V (2019) Undrained cyclic laboratory behaviour of sandy soils. Geosciences, 9, 512: 1–27

Cavallaro A, Ferraro A, Grasso S. and Maugeri M (2008) Site response analysis of the Monte Po Hill in the City of Catania. Proceedings of the 2008 Seismic Engineering International Conference, Reggio Calabria and Messina, 2008, AIP Conference Proceedings, 1020(PART 1): 583–594

Cavallaro A, Abate G, Ferraro A, Giannone A, Grasso S (2019) Seismic slope stability analysis of rainfall-induced landslides in Sicily (Italy). Proceedings of the 7th International Conference on Earthquake Geotechnical Engineering, Roma, 1672-1680

Clough RW, Penzien J (1975) Dynamics of structures. McGraw-Hill, New York

Conte E, Dente G, Ausilio E (2000) Seismic stability analysis of reinforced slopes. Soil Dyn Earthq Eng 19(3):159–172

Dawson EM, Roth WH, Drescher A (1999) Slope stability analysis by strength reduction. Géotechnique. 49(6):835–840

Duncan JM (1996) State of the art: limit equilibrium and finite-element analysis of slopes. Journal of Geotechnical Engineering, ASCE. 122(7): 577–596

Fredlund DG, Krahn J (1977) Comparison of slope stability methods of analysis. Can Geotech J 14(3):429–439

Goren L, Aharonov E, Anders HM (2010) The long runout of the Heart Mountain landslide: heating, pressurization, and carbonate decomposition. J Geophys Res 115:B10

Griffiths DV (2015) A guide to the use of program slope64. USA, Colorado School of Mines

Griffiths DV, Lane PA (1999) Slope stability analysis by finite elements. Géotechnique. 49(3):387–403

Gupta AK (1990) Response spectrum method in seismic analysis and design of structures. Blackwell Scientific Publications Inc., USA

Hardin BO, Drnevich VP (1972a) Shear modulus and damping in soils: measurement and parameter effects. Journal of the Soil Mechanics and Foundations Division, ASCE. 98(6): 603–624

Hardin BO, Drnevich VP (1972b) Shear modulus and damping in soils: design equations and curves. Journal of the Soil Mechanics and Foundations Division, ASCE. 98(7): 667–692

Huang HW, Wen SC, Zhang J et al (2018) Reliability analysis of slope stability under seismic condition during a given exposure time. Landslides. 15:2303–2313

ITASCA Consulting Group Inc (2015) FLAC–fast Lagrangian analysis of continua, version 8.0, USA: Minneapolis

Janbu NL (1954) Application of composite slip surfaces for stability analysis. In: Proc. European Conf. on Stability of Earth slopes, Stockholm

Jibson RW (2011) Methods for assessing the stability of slopes during earthquakes—a retrospective. Eng Geol 122(1):43–50

Johnson GR (2011) Numerical algorithms and material models for high-velocity impact computations. International Journal of Impact Engineering. 38(6): 456–472

Leshchinsky D, San KC (1994) Pseudostatic seismic stability of slopes: design charts. J Geotech Eng Div 120(9):1514–1532

Li AJ, Lyamin AV, Merifield RS (2009a) Seismic rock slope stability charts based on limit analysis methods. Comput Geotech 36(1–2): 135–148

Li AJ, Merifield RS, Lyamin AV (2009b) Limit analysis solutions for three dimensional undrained slopes. Comput Geotech 36(8):1330–1351

Lin CW, Shieh CL, Yuan BD et al (2003) Impact of Chi-Chi earthquake on the occurrence of landslides and debris flows: example from the Chenyulan River watershed, Nantou, Taiwan. Engineering Geology. 71(1–2): 49–61

Liu J, Liang X, Xue Y, Yao K, Fu Y (2020) Numerical evaluation on multiphase flow and heat transfer during thermal stimulation enhanced shale gas recovery. Appl Therm Eng 178:115554

Morgenstern NR, Price VE (1965) The analysis of the stability of general slip surfaces. Géotechnique. 15(1):79–93

Newmark NM, Hall WJ (1982) Earthquake spectra and design. Earthquake Engineering Research Institute, Berkeley

Nouri H, Fakher A, Jones C (2006) Development of horizontal slice method for seismic stability analysis of reinforced slopes and walls. Geotext Geomembr 24(3):175–187

Piero G (2012) Help documentation of SIMQKE_GR version 2.7. Italy, University of Brescia

Sarma SK (1979) Stability analysis of embankment and slopes. Journal of Geotechnical Engineering Division ASCE 105(12):1511–1524

Schnabel PB, Lysmer J Seed HB (1972) SHAKE: a computer program for earthquake response analysis of horizontally layered sites. Earthquake Engineering Research Center, University of California, Berkeley, California

Seed HB, Wong RT, Idriss IM et al (1986) Moduli and damping factors for dynamic analyses of cohesionless soils. Journal of the Geotechnical Engineering Division ASCE 112(11):1016–1032

Seismosoft (2016) Help Documentation of SeismoSignal 2016 released. USA: Seismosoft Ltd

Shukha R, Operstein V, Frydman S (2006) Stability charts for pseudo-static slope stability analysis. Soil Dyn Earthq Eng 26(9):813–823

Simulia DS (2017) Abaqus 6.17 help documentation. Dassault Systems Corp

Spencer E (1967) A method of analysis of stability of embankments assuming parallel interslice forces. Géotechnique 17(1):11–26

State Economic and Trade Commission, PRC. (2000) Code for seismic design of hydraulic buildings (Power industry standard of the People's Republic of China)

Sun JI, Golesorkhi R, Seed HB (1988) Dynamic moduli and damping ratios for cohesive soils, Earthquake Engineering Research Center, University of California, Berkeley, Report NO. UCB/EERC-88/15

Tang C, Zhu J, Li WL et al (2009) Rainfall-triggered debris flows following the Wenchuan earthquake. Bull Eng Geol Environ 68:187–194

Travasarou T, Bray JD (2009) Pseudostatic coefficient for use in simplified seismic slope stability evaluation. J Geotech Geoenviron 135(9):1336–1340

Xue Y, Teng T, Dang FN, Ma ZY et al (2020) Productivity analysis of fractured wells in reservoir of hydrogen and carbon based on dual-porosity medium model. Int J Hydrog Energy 45(39):20240–20249

Yin YP, Wang FW, Sun P (2009) Landslide hazards triggered by the 2008 Wenchuan earthquake, Sichuan,China. Landslides 6:139–151

Yin YP, Zheng WM, Li XC et al (2011) Catastrophic landslides associated with the M8.0 Wenchuan earthquake. Bull Eng Geol Environ 70:15–32

Zienkiewicz OC, Humpheson C, Lewis RW (1975) Associated and non-associated visco-plasticity and plasticity in soil mechanics. Géotechnique. 25(4):671–689